Prepared for the National Institutes of Health
National Institute of Neurological Disorders and Stroke
Division of Fundamental Neurosciences
Neural Prosthesis Program
Bethesda, MD 20892

Unassisted Standing with Functional Neuromuscular Stimulation

NIH-NINDS-N01-NS-6-2351

Progress Report #9

Period Covered:
January 1, 1999 – March 31, 1999

Principal Investigator: Ronald J. Triolo, Ph.D.[1]
Co-Principal Investigators: Robert F. Kirsch, Ph.D.[2]
John A. Davis, Jr., M.D.[1]

Departments of Orthopaedics[1] and Biomedical Engineering[2]
Case Western Reserve University
Cleveland, OH 44106-4912

Co-Investigators: James J. Abbas, Ph.D.
University of Kentucky

Scott L. Delp, Ph.D.
Stanford University

INTRODUCTION

The long-term goal of this contract is to develop methods to provide brace-free, energy efficient standing for persons with complete thoracic level spinal cord injuries via functional neuromuscular stimulation (FNS). The resulting system will resist reasonable disturbances and maintain balance automatically while allowing free use of the upper extremities to manipulate objects in the environment. These objectives are being addressed through an organized effort consisting of anatomical and dynamic modeling, control simulation and optimization, and experimental demonstration of new control structures. The work represents an active partnership between investigators at Case Western Reserve University (CWRU) and collaborators at Northwestern University (NU) and the University of Kentucky (UK).

PROGRESS THIS REPORTING PERIOD

Efforts this quarter have concentrated on a) completing the final version of the model of the musculoskeletal anatomy of the trunk, b) integrating passive joint properties into the dynamic 3D bipedal computer model of human stance, and c) simulation of feed-forward and preparatory postural control systems. This report summarizes these results and their relationship to the goals of the contract.

A. Incorporating the Actions of the Trunk: Anatomical Modeling of the Torso

Controlling the mass of the trunk is critical to erect posture and the maintenance of balance. The objective of this component of the contract was to measure directly the key anatomical parameters of the prime movers of the trunk that are accessible to electrical stimulation. These measurements were then used to develop a computational model of the biomechanics of the torso that were combined with our existing model of the pelvis and lower extremities to predict the effects of electrical stimulation test various control strategies in simulation. This following section represents the final report of our efforts to model the trunk and incorporate it into our three dimensional simulation of human posture.

Previous quarterly progress reports described the dissection protocol and analysis techniques employed to determine the architecture of the trunk muscles of interest (**rectus abdominus, quadratus lumborum** and **erector spinae**). Over the past three months, detailed analyses were completed on the last sets of muscle specimens. In total, specimens from five cadavers (four fresh-frozen and one embalmed) were analyzed and the resulting architectural parameters were pooled to construct the final computational model of the actions of the trunk. Anthropometric data for each cadaver are summarized in **Table I** to represent their relative size.

All cadaver specimens were in a neutral position during dissection, and harvested muscles were preserved in 10% formaldehyde solution. Each muscle was treated with phosphate buffer to neutralize the formalin and placed in 15% sulfuric acid for 24-48 hours to remove fat and unwanted fascia. It was then rinsed in phosphate buffer once again to neutralize the acid (Sacks and Roy, 1982). Overall muscle geometry (musculotendon length) with the muscle intact

and *in situ* in the cadaver, after dissection, and after fixing in formalin indicated a small change of less than two centimeters in all specimens. This is in agreement with other studies showing little shrinkage (<2%) due to fixing the tissue (Cutts, 1988)

Table I: Anthropometric data for all cadaver specimens

Specimen	Age (yr)	Sex	Height (cm)	Weight (kg)
1	-	F	169	69.1
2	-	F	169	95.5
3	68	M	177	68.2
4	57	M	172	74.1
5*	75	F	166	65.9
Mean (S.D.)	66.7 (9.1)	3 female, 2 male	170.6 (4.2)	76.2 (13.3)

* - Specimen 5 was embalmed, specimens 1 - 4 were fresh frozen

The erector spinae and the quadratus lumborum were subdivided into multiple components. The erector spinae was represented by **spinalis thoracis**, **longissimus thoracis** (thoracic fibers), and the **iliocostalis lumborum** (thoracic fibers). The quadratus lumborum was divided into two components: a **proximal** component and a **distal** component. The proximal component represented average of the fibers attaching into the 12th rib and the L1 vertebra, while the distal component represented the average of the fibers attaching to the L2-L4 vertebrae.

Musculotendon length, muscle length, fascicle length, pennation angle, sarcomere length and muscle mass were measured for each specimen. From these parameters, physiological cross-sectional areas (PCSA) and optimal fiber lengths were derived. The musculotendon length was measured as the distance between the attachments of the most proximal most distal tendons. The muscle length was defined as the distance between the proximal tip of the most proximal fiber and the distal tip of the most distal fiber. Fascicle length was defined as the length of an individual fascicle traced from origin to its insertion. Pennation angle was defined as the angle made by the fibers with the line of action defined for the muscle. Sarcomere length was estimated using a laser diffraction method (Yeh et al., 1980 and Baskin et al.,1981). From the fascicle and sarcomere lengths, an approximate number of sarcomeres per fascicle was derived, which when multiplied by the optimum sarcomere length for mammalian muscle (2.8 μm), yielded the estimate for optimal fascicle length. The muscle fiber volume was estimated as the ratio of the muscle fiber mass and a muscle density value of 1.06 g/cm^2 (Mendez and Keys, 1960), and PCSA was calculated as the ratio of the muscle fiber volume and fascicle length.

The final values of the model parameters are summarized in **Table II** below. Although there were some variations in the size of the specimens, the muscle parameters measured were consistent across the specimens. The variation in musculotendon length for all the muscles was less than 15%, and muscle length varied by less than 25%. Mean sarcomere length was consistent within individual specimens, although measurements varied from cadaver to cadaver (ranging from 1.89 μm to 3.59 μm for rectus abdominus). The muscle masses varied considerably, up to 60% of the means.

Table II: Mean muscle architectural parameters from all cadaver specimens*

Muscle		MT	ML	PA	FL	SL	OFL	MFM	PCSA
Quadratus Lumborum	*(proximal)*	11.7 (1.7)	10.7 (1.3)	7.4 (2.9)	7.3 (1.3)	2.39 (0.21)	8.5 (1.5)	13.3 (5.2)	1.55 (0.58)
	(distal)	9.3 (1.3)	8.1 (1.2)	7.4 (6.2)	4.7 (0.5)	2.37 (0.20)	5.6 (0.9)	7.35 (2.4)	1.24 (0.45)
Erector Spinae	*Spinalis Thoracis*	24.7 (1.5)	18.2 (3.2)	16.0 (3.8)	5.2 (0.4)	2.26 (0.17)	6.4 (0.6)	10.24 (6.0)	1.55 (0.96)
	Iliocostalis Thoracis	42.6 (5.5)	34.7 (4.8)	12.6 (5.8)	9.6 (1.2)	2.31 (0.17)	11.7 (2.1)	73.43 (31.0)	5.93 (2.55)
	Longissimus Thoracis	43.8 (4.3)	33.1 (9.0)	13.8 (4.5)	12.0 (1.7)	2.37 (0.17)	14.2 (2.1)	60.96 (29.9)	4.08 (1.99)
Rectus Abdominus		35.9 (1.9)	24.3 (2.7)	0.0 (0.0)	28.3 (3.6)	2.83 (0.28)	28.0 (4.2)	92.5 (30.5)	2.64 (0.97)

MT: Musculotendon length (cm)
ML: Muscle length (cm)
PA: Pennation angel (degrees)
FL: Fiber length (cm)
SL: Sarcomere length (um)
OFL: Optimal fiber length (cm)
MFM: Muscle Fiber Mass (gm)
PCSA: Physiological cross sectional areas (cm^2)

* - Mean (Standard Deviation) for N=5

Table III compares the PCSA values estimated in this study to others reported in the literature. The anatomically based PCSAs indirectly derived in this study are consistently lower in all the muscles compared to values estimated from imaging studies. This may be due to the fact that the specimens in this investigation were from elderly individuals, rather than the normal younger volunteers used in most imaging studies. In addition, not all the components of the erector spinae (such as the multifidus and lumbar ilocostalis and longissimus) were included in our calculations of muscle mass, and imaging techniques used to estimate PCSAs often report average cross sectional areas based on only a few vertebral levels.

Table III: Comparison of PCSA (cm^2) estimates to previously published reports

	Present Study[a]	Bogduk et al., 1992[a]	Reid & Costigan, 1985[b]	McGill et al., 1988[b]	Tracy et al., 1989[b]	Chaffin et al., 1990[b]	Han et al., 1992[b]	Tsuang et al., 1993[b]
Rectus Abdominus	2.64	-	10.50	7.90	6.85	3.80	4.90	6.94
Quadratus Lumborum	2.79	-	-	6.10	6.43	4.20	2.62	5.00
Erector Spinae	11.56	16.55	15.88	-	20.03	18.05	12.89	16.46

[a]PCSA values estimated by anatomical studies
[b]PCSA values estimated from radiographs, CT, or, MRI imaging.

These architectural parameters characterize the force producing capacities of each muscle. The mechanical relationships of the muscles to the skeleton have also been finalized, and the flexion, bending and rotation of the torso in response to the forces produced by these muscles can now be computed. The definition of a 3D model of the human trunk using the SIMM (Software for Interactive Musculoskeletal Modeling, Musculographics, Inc.) software tool was completed this reporting period, as illustrated in **Figure 1**. Preliminary origin and insertion points of the erector spinae, quadratus lumborum, and rectus abdominus determined from anatomical drawings and CT/MRI images were confirmed in our dissection studies.

Figure 1: 3D Model of the trunk with representations of three trunk muscles

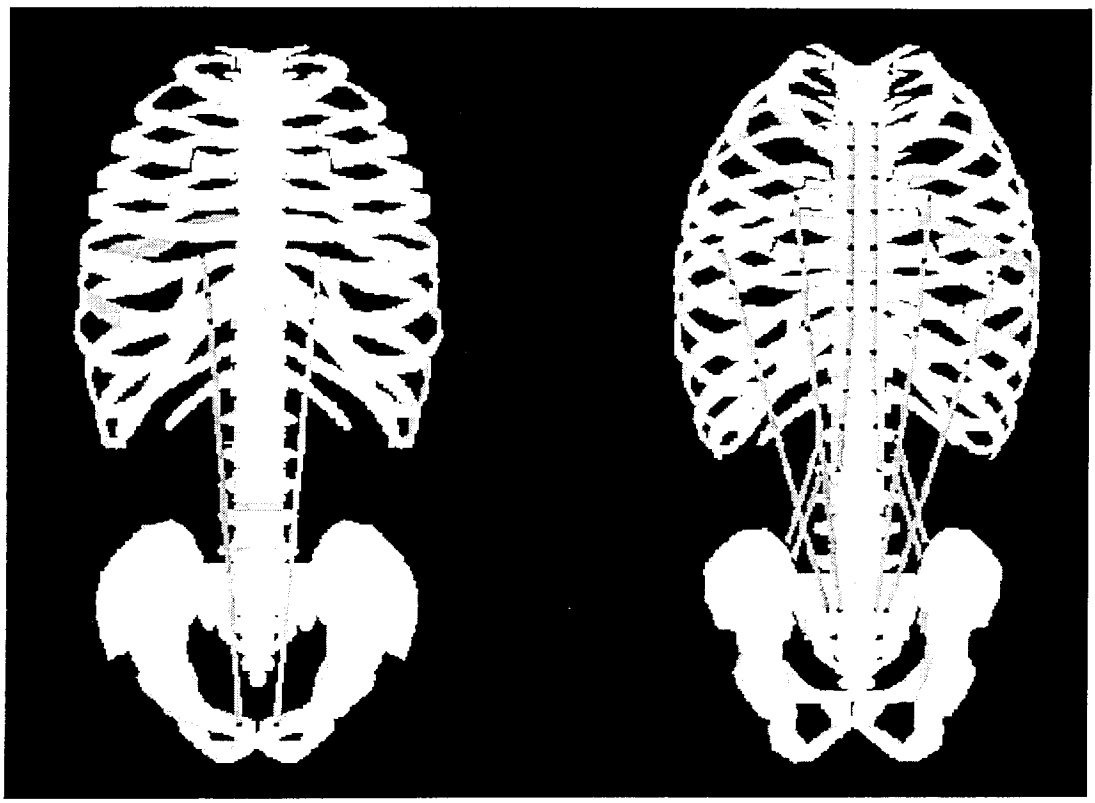

The digitized model of the spine (obtained from Viewpoint Imaging) consists of 3D surface representations (polygonal form) of the bones. In accordance with the anatomical study described above, the representation of the iliocostalis lumborum, the most lateral column of the erector spinae, originates from the sacrum and inserts into the angle of the 7^{th} rib. The longissimus thoracis, the middle column, originates from the sacrum and inserts into the 6^{th} rib. The spinalis thoracis, the most medial column, originates at the transverse process of the L2 vertebra and inserts into the T2 vertebra. The proximal component of the quadratus lumborum originates from the iliac crest and inserts into the L1 vertebra. The distal component also originates from the iliac crest but inserts into the L2 vertebra. The rectus abdominus originates from the pubic symphysis and inserts into the cartilage of the 6^{th} rib.

The moment arms of each of the muscles in the sagittal plane (anterior-posterior direction) and at each vertebral level at the neutral spine posture were computed for the model and compared against values estimated with radiographic, CT and MRI imaging techniques as reported in the literature (Kumar, 1998; Tracy et al., 1989; Chaffin et al., 1990; Bogduk et al., 1992; Moga et al., 1993; Tsuang et al., 1993). **Table IV** summarizes these results for all three muscle groups in the lumbar area. The values for the erector spinae are averages of the three columns. As evident in the table, there is good agreement between the moment arms represented in the model with previously published reports.

Table IV: Moment arms (cm) derived from our model compared to previously published values

	MODEL	Moga et al. 1993	Tracy et al. 1989	Kumar 1988	Tsuang et al. 1993	Chaffin et al. 1990	Bogduk et al. 1992
				Erector Spinae			
L1 – L2	6.4	5.0	-	-	-	-	4.7
L2 – L3	6.9	5.0	5.8	-	5.2	5.4	5.2
L3 – L4	6.7	5.3	5.8	5.9	4.9	5.3	5.8
L4 – L5	5.8	5.1	6.0	-	4.9	5.3	5.3
L5 – S1	3.9	-	6.2	5.9	-	-	3.9
				Quadratus Lumborum			
L1 – L2	2.4	3.0	-	-	-	-	
L2 – L3	2.8	3.3	3.5	-	3.2	3.5	
L3 – L4	3.2	3.2	3.2	3.8	2.8	3.2	
L4 – L5	2.8	2.8	2.8	-	-	2.8	
L5 – S1	2.5	-	-	2.8	-	-	
				Rectus Abdominus			
L1 – L2	10.1	13.5	-	-	-	-	
L2 – L3	8.5	12.2	8.7	-	7.0	7.1	
L3 – L4	7.4	11.0	8.0	10.7	6.3	7.1	
L4 – L5	7.0	10.5	7.4	-	6.1	7.0	
L5 – S1	7.7	-	8.1	10.6	-	-	

As previously reported, the kinematics for flexion-extension (pitch), lateral bending (roll), and axial rotation (yaw) of the spine have also been developed. The motion of the spine was distributed among the various vertebral levels as described by White and Panjabi (1990). The center of rotation for individual vertebral bodies was based on study by Pearcy and Bogduk (1988).

This new model of the human torso has been integrated into the three dimensional model of the lower limbs and pelvis. The complete musculoskeletal model will be employed in coming contract periods to perform the investigative simulations required to design and study various FNS control systems to automatically maintain standing posture and balance. Two peer-reviewed publications are in preparation as a result of this component of the contract.

B. Incorporating Passive Joint Properties

The objective of this part of the contract is to determine the influence of the passive moments developed at the joints of the lower extremities in individuals with SCI on the ability to maintain balance and upright posture, and to complete maneuvers such as the as sit-to-stand transitions. Understanding the relationship between the passive joint moments and those actively generated by stimulated muscle contractions will allow us to design more realistic automatic postural control systems. The goal is to develop both control strategies that work in concert with the passive joint properties by compensating for passive moments that oppose a desired joint movement, and exploiting passive properties that act in the same direction as the desired movement or that help maintain a stable standing posture. Currently, our 3D biomechanical model of human stance does not include a representation of the passive joint properties, which are likely to change significantly as a result of spinal cord injury. Incorporating passive joint properties into the model will allow us to address these issues in simulation to avoid testing inefficient control strategies that do not complement the existing

Elasticity and viscoelasticity are the two most dominant properties of human joints. Several investigators (Yoon and Mansour, 1982; Esteki and Mansour, 1996; Riener and Edrich, 1997) have used exponential functions to model the elastic component of passive joint moment. These models have been functions of the joint angle of interest, as well as the positions of adjacent joints to describe the mechanical coupling between joints due to biarticular muscles. The viscoelastic component dissipates energy as a function of the joint velocity. As a result, the curve relating moment and joint angle exhibits a velocity dependent hysteresis loop. In the past, researchers have either ignored this viscoelastic hysteresis (Reiner and Edrich, 1997) or represented it with two separate equations (Yoon and Mansour, 1982; Esteki and Mansour, 1996). In the latter approach, one equation models the upper portion of the hysteresis loop as the joint moves in one direction, while the second equation models the lower portion as the direction of motion is reversed. As a consequence, two sets of model parameters need to be identified, as well as a method to switch between equations as the direction of movement changes, thus complicating the performance of computer simulations.

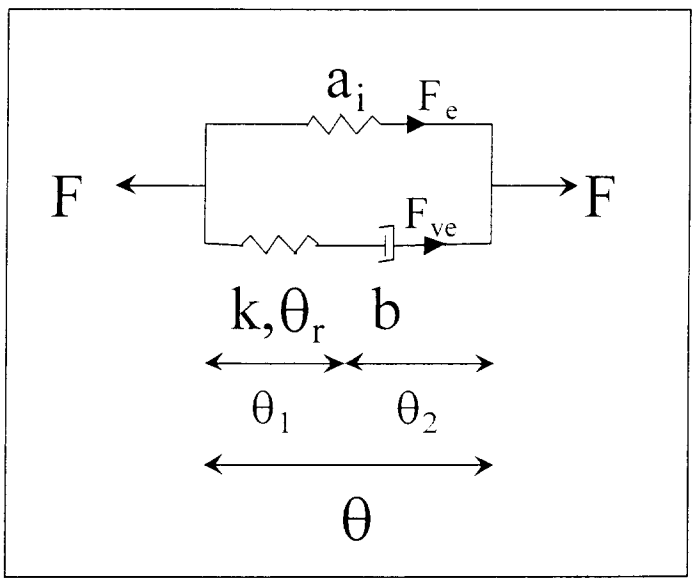

Figure 2: Model for passive moment based upon the Kelvin representation for viscoelasticity. The mathematical relationship models the actual moment directly related to the force through the moment arm.

Figure 2 illustrates the model that has been developed to eliminate the need for two equations by describing both the elastic and viscoelastic properties of a joint in a single mathematical relationship. The equation is based upon the Kelvin model for viscoelasticity. The model consists of

an elastic element in parallel with an elastic and viscous element in series. The single elastic element represents the elastic component of the passive properties; therefore it has been modeled as a combination of two exponential functions. The elastic and viscous element in series represent the viscoelastic component. The elastic element is modeled as a linear spring, and the viscous element is modeled as a quasi-linear dashpot. The equations to describe the moments generated by each of these elements are:

$$M_{elastic} = a_1 e^{a_2\theta + a_3\theta_p + a_4\theta_d} - a_5 e^{a_6\theta + a_7\theta_p + a_4\theta_8} + a_9$$

$$M_{viscoelastic} = -k(\theta_1 - \theta_r) = -b\dot{\theta} + c_1 \operatorname{sgn}(\dot{\theta}) + c_2 (\operatorname{sgn}(\dot{\theta}))^2$$

θ = joint angle

θ_p and θ_d = proximal and distal joint angles respectively

θ_r = neutral joint angle for the linear elastic element

a_i, k, b, c_1, and c_2 are parameters which will be estimated from experimental data

Graphical representations for each of these equations are shown in **Figure 3**. Using a model of this form allows us to model the passive joint moment developed when the joint is moving (according to the classical viscoelastic hysteresis) as well as the decay of the passive moment when the joint is held fixed. Using this model, the following differential equation was developed:

$$M + \tau_e \dot{M} = M_e + b\left(\frac{\dot{M}_e}{k} - \dot{\theta}\right) + c_1 \operatorname{sgn}(\dot{\theta}) + c_2 (\operatorname{sgn}(\dot{\theta}))^2$$

$$\tau_e = \frac{b}{k}$$

For implementation into computer simulations, the following numerical solution to the above equation was derived:

$$M_{n+1} = M_n + hg$$

$$g = {}^{1}\!/_{\tau_e}\left[M_{e_n} + b\left(\frac{\dot{M}_{en}}{k} - \dot{\theta}_n\right) + c_1 \operatorname{sgn}(\dot{\theta}_n) + c_2 (\operatorname{sgn}(\dot{\theta}_n))^2 - M_n\right]$$

$$\dot{M}_{en} = a_1 e^{a_2\theta + a_3\theta_p + a_4\theta_d}\left(a_2\dot{\theta}_n + a_3\dot{\theta}_{p_n} + a_4\dot{\theta}_{d_n}\right) - a_5 e^{a_6\theta + a_7\theta_p + a_4\theta_8}\left(a_6\dot{\theta}_n + a_7\dot{\theta}_{p_n} + a_7\dot{\theta}_{d_n}\right)$$

$$\dot{\theta} = \frac{\theta_n - \theta_{n-1}}{h}$$

h = *step size*

The numerical solution described above was implemented at the ankle of our 3D biomechanical model of the lower extremities in SIMM. As a preliminary verification of this model of passive joint properties, computer simulations were performed for the ankle joint and the results compared to experimental data.

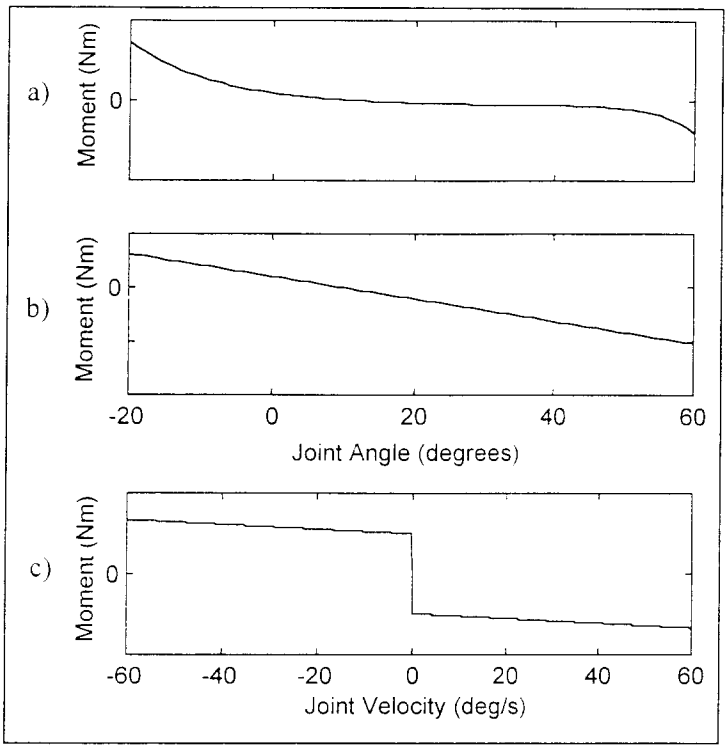

Figure 3: Graphical representations of the equations for the elastic and viscoelastic elements of the model. a) Non-linear elastic element, b) Linear elastic element and c) Quasi-linear viscous element. The parameters c1 and c2 provide an offset for the viscous element. This form provides a minimal level of viscosity for all velocities.

Simulations consisted of passively rotating the representation of the ankle joint throughout its range of motion at three different velocities (10, 50 and 100 degrees per second). The parameters of the model for these simulations were derived from the literature. The nonlinear elastic elements were based upon the values reported by Reiner and Edrich (1997), and parameters for the viscoelastic elements were extrapolated from Esteki and Mansour (1996). Experimental data were obtained from able-bodied volunteers using a KinCom 500H robotic dynamometer as described in previous progress reports. The testing protocol consisted of preconditioning the joint by cycling it through its range of motion 20 times. Preconditioning ensured that the measurements would not be dependent upon the previous positions of the joint. Following the preconditioning the ankle was passively rotated through its range of motion for 10 cycles. Testing was repeated at the same three velocities used in simulation.

The simulation and experimental results for a velocity of 50 degrees per second are plotted in **Figure 4**. For each curve the upper trace represents a movement from dorsiflexion (negative joint angles) to plantarflexion (positive joint angles). The bottom traces for each curve represent a movement in the opposite direction. Qualitatively the curves have similar shapes. These results were consistent from cycle to cycle at each of the velocities tested. Differences between the simulated and experimental curves may be attributed to the fact that the parameters of the model were taken from the literature and not calculated directly from experimental data for the ankle joint.

Summary and future plans: A general model to describe the passive moment produced at a joint has been developed. The model incorporates elastic as well as viscoelastic properties therefore negating the need for two equations to model the effects of hysteresis. Using

parameters from the literature, computer simulations were compared to experimental data obtained for the ankle. The results indicate that the model should be able to properly account for the relevant components of the passive moment. However model parameters will need to be determined using appropriate experimental data. Future experimental data will be obtained from able-bodied individuals and individuals with spinal cord injuries. Having an appropriate model for both subjects groups will enable us to investigate the changes that occur after a spinal cord injury.

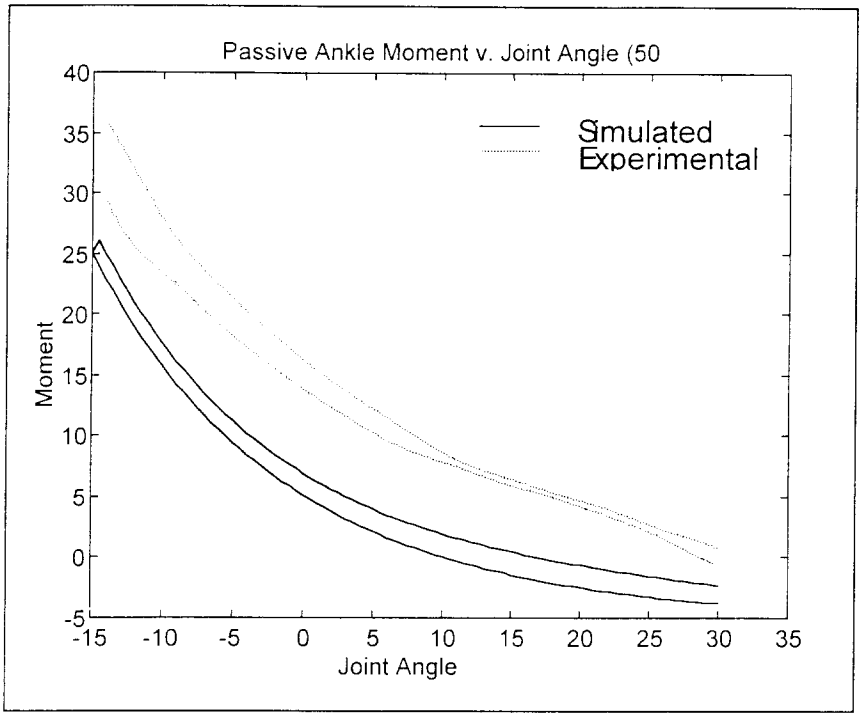

Figure 4: Comparison of simulated passive moments at the ankle joint as predicted by the Kelvin model implemented in SIMM with experimental data collected under the same conditions.

C. Feedforward and Preparatory Control System Development

One component of our proposed control system will provide users with the ability to set and make adjustments to their posture in preparation of a disturbance or in response to fatigue. A major concern with this approach to the command/control interface is that the nonlinearities of the musculoskeletal system may make it difficult for the person to make the desired adjustments. A large part of our work is directed at characterizing the effect of these nonlinearities and at compensating for them. Primary accomplishments to this end during this contract period were 1) completion of a real-time simulation system to investigate the effects of nonlinear system properties on user-input control, 2) incorporation of an adaptive neural algorithm for linearizing input/output properties into the software for model-based studies and for real-time controller implementation. We have continued the model-based studies using this algorithm.

Real-time simulation of posture control: The objective of this work was to develop a real-time simulation of posture control. In this system, the user views a graphical display on the computer monitor and interacts with the model in real-time to adjust posture. This system will be used to: 1) characterize the effects of system nonlinearities on the user's ability to make adjustments to standing posture, 2) evaluate the ability of the adaptive control system to linearize input/output properties, and 3) to determine if the adaptive control system improves the user's ability to make adjustments.

A LabVIEW-based software system has been developed which incorporates operator input, adaptive neural network filtering, a detailed musculoskeletal model, and a graphical video display. The user balances an inverted pendulum by differentially controlling simulation to an antagonist muscle pair using a standard input device, such as a joystick. The muscle model includes nonlinear recruitment, muscle activation dynamics, muscle activation delay, as well as torque-angle, and torque-velocity properties. A neural network can be used as an adaptive co-stimulation map to relate operator input to muscle activation. The user-controlled simulation system has been developed for real-time operation on a Pentium-based PC.

Figure 5 presents data for an instantaneous linear torque generator plant and a plant including nonlinear muscles with a fixed bilinear co-stimulation map. This example demonstrates that the system nonlinearities degrade the user's ability to maintain upright posture.

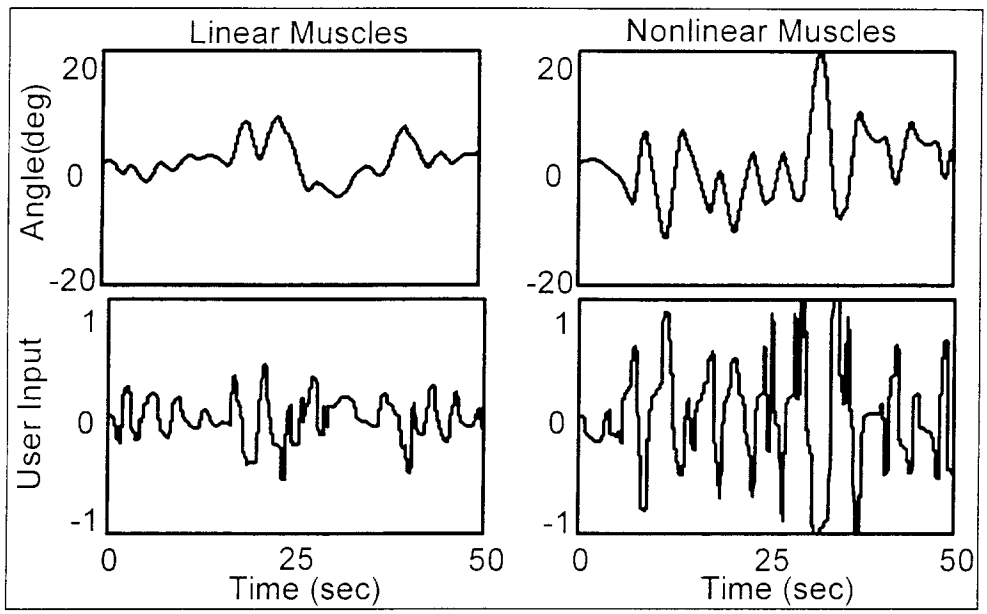

Figure 5: Joint Angle and User Input versus time for linear and nonlinear muscle models. The nonlinear system was less accurately controlled and required more active user input. The musculoskeletal model represents coronal plane posture influenced by the left and right abductor muscles. The neural network was not used in these trials.

Adaptive filtering to linearize system input/output properties: In previous work, we had developed an adaptive neural network filtering algorithm for use in the user-adjustment component of the control system. In this configuration, the neural network filter acts as an adaptive map to translate user input to stimulation values. The objective of this adaptive filter is to linearize the input/output properties as seen by the user (i.e. to linearize the relationship between the signal provided by the user and the joint angle output).

The adaptive map utilizes a 2-layer feedforward function approximation neural network algorithm that uses a constrained learning algorithm in order to facilitate rapid learning. The first layer of neurons uses sigmoid transfer functions with biases adjusted so that the sensitivity

regions span the input range. The output neuron uses a linear threshold, and the learning rule adjusts the weights on the output neuron as a function of output error, neural activity level, and learning rate.

Evaluation of the algorithm on a simplified musculoskeletal model was described in previous quarterly progress reports, which demonstrated that the system was able to account for both recruitment nonlinearities and on-line changes in muscle properties due to fatigue. In this contract period, we have developed C-code versions of the adaptive control system software and we have interfaced this code with musculoskeletal models developed in SIMM and SD/FAST. A non-linear model of muscle recruitment property was also incorporated into the SIMM-SD/FAST model. In addition, the C-code for the adaptive neural network has been incorporated into our LabVIEW-based software system for real-time FNS control.

In an initial series of simulations, user input was modeled as a slow ramp and sent through the adaptive neural network filter to the musculoskeletal model. Muscle model parameters (including recruitment properties and muscle strength) and filter parameters (network size and learning rate) were varied. These initial simulations are consistent with the results of our previous studies on simpler musculoskeletal models. The adaptive filter has been able to account for nonlinear musculoskeletal properties and provide the user with an overall system that is more linear and easier to control.

Summary and immediate plans: In this contract period we have developed a real-time simulation system and we have continued evaluation of the adaptive neural network component of the control system. A series of studies using the real-time simulation system are planned for the next contract period. The goals will be to: (1) determine the effect of muscle properties on the operator's ability to complete the desired task, (2) determine whether the adaptive filter can account for these muscle properties, and (3) determine if the adaptive controller improves the user's ability to make adjustments. The performance of the adaptive neural network system will be further characterized in model-based studies using SIMM/SDFAST and eventually in experiments on human subjects.

Publications resulting from work this contract period:

Papers:

[1] Suryanarayanan S., Delp S., Murray W., Uhlir J., Triolo R.. Architectural parameters of trunk muscles. *Journal of Biomechanics* – (submitted).

[2] Werner K.N., Triolo R.J., Kirsch R.F. Modeling the postural disturbances caused by upper extremity movements. *Journal of Biomechanics* – (submitted)

[3] Uhlir J.P., Triolo R.J., Peckham P.H., Crago P.E., Mansour J.M., Kobetic R. The use of selective stimulation of the quadriceps to improve standing function in paraplegia. *IEEE Transactions on Rehabilitation Engineering* – (submitted)

[4] Triolo R.J., Bogie K. Lower extremity applications of functional neuromuscular stimulation after spinal cord injury. *Journal of SCI Rehabilitation* – (submitted).

Abstracts:

[1] Hartman E., Triolo R.J., Abbas J. Effects of system nonlinearities on posture adjustments using functional neuromuscular stimulation. *Proceedings, IEEE Engineering in Medicine and Biology Society*, Atlanta GA, 1999 – (in press).

[2] Zhang X., Triolo R.J., Abbas J. Task-dependent adjustments to co-stimulation levels in functional neuromuscular stimulation systems. *Proceedings, IEEE Engineering in Medicine and Biology Society*, Atlanta GA, 1999 – (in press).

REFERENCES

Baskin, R.J., Lieber, R.L., Oba, T., Yeh, Y., 1981. Intensity of light diffraction from striated muscle as a function of incident angle. *Biophysical Journal* 36, 759-773.

Bogduk, N., Macintosh, J.E., Pearcy, M.J., 1992. A universal model of the lumbar back muscles in the upright position. *Spine* 17, 897-913.

Chaffin, D.B., Redfern, M.S., Erig, M., Goldstein, S.A., 1990. Lumbar muscle size and locations from CT scans of 96 women of age 40 to 63 years. *Clinical Biomechanics* 5, 9-16.

Cutts, A., 1988. Shrinkage of muscle fibers during the fixation of cadaveric tissue. *Journal of Anatomy* 8, 160-175.

Esteki A., Mansour J.M., 1996. An experimentally based nonlinear viscoelastic model of joint passive moment, *Journal of Biomechanics*, 29:443-450.

Han, J.S., Ahn, J.Y., Goel, V.K., Takeuchi, R., McGowan, D., 1992. CT-based geometric data of human spine musculature. Part I. Japanese Patients with Chronic low back pain. *Journal of Spinal Disorders* 5(4), 448-458.

Kumar, S., 1988. Moment arms of spinal musculature determined from CT scans. *Clinical Biomechanics* 3, 137-144.

McGill, S.M., Patt. N., Norman. R.W., 1988. Measurement of the trunk musculature of active males using CT scan radiography: implications for force and moment generating capacity about the L4/L5 joint. *Journal of Biomechanics* 21(4), 329-341.

Mendez, J., Keys, A., 1960. Density and composition of mammalian muscle. *Metabolism* 9, 184-188.

Moga, P.J., Erig, M., Chaffin, D.B., Nussbaum, M.A., 1993. Torso muscle moment arms at intervertebral levels T10 through L5 from CT scans on eleven male and eight female subjects. *Spine* 18(15), 2305-2309.

Pearcy, M.J., Bogduk, N., 1988. Instantaneous axes of rotation of the lumbar intervertebral joints. *Spine* 13(9), 1033-41.

Reid, J.G., Costigan, P.A., 1985. Geometry of adult rectus abdominus and erector spinae muscles. *Journal of Orthopaedics and Sports Physical Therapy* 6, 278-280.

Riener R., Edrich T. , 1997. Significance of passive elastic joint moments in FES, *Proc. Second Ann. IFESS Conf.*, 103-106.

Sacks, R.S., Roy, R.R., 1982. Architecture of the hind limb muscles of cats: Functional significance. *Journal of Morphology* 173, 185-195.

Tracy, M.F., Gibson, M.J., Szypryt, E.P., Rutherford, A., Corlett, E.N., 1989. The geometry of the muscles of the lumbar spine determined by magnetic resonance imaging. *Spine* 14(2), 186-193.

Tsuang, Y.H., Novak, G.J., Schipplein, O.D., Hafezi, A., Trafimow, J.H., Anderson, G.B., 1993. Trunk muscle geometry and centroid location when twisting. *Journal of Biomechanics* 26(4/5), 537-546.

White, A.A., Panjabi, M.M., 1990. Clinical Biomechanics of the Spine. 2nd edition, J.B. Lippincott Company, Philadelphia.

Yeh, Y., Baskin. R.J., Lieber, R.L., Roos, K.P., 1980. Theory of light diffraction by single skeletal muscle fibers. *Biophysical Journal* 29, 509-521.

Yoon Y.S., Mansour J.M. , 1982. The passive elastic moment at the hip, *Journal of Biomechanics*, 15:905-910.